Surface & Coatings Technology 206 (2011) 434–439

Contents lists available at ScienceDirect

Surface & Coatings Technology

journal homepage: www.elsevier.com/locate/surfcoat

Tribological behavior under aggressive environment of diamond-like carbon films with incorporated nanocrystalline diamond particles

F.R. Marciano [a,b,*], R.P.C. Costa [b,c], D.A. Lima-Oliveira [b,d], A.O. Lobo [a,b], E.J. Corat [b], V.J. Trava-Airoldi [b]

[a] Instituto de Pesquisa e Desenvolvimento (IP&D), Universidade do Vale do Paraíba, Av. Shishima Hifumi 2911, São José dos Campos, SP, Brazil
[b] Laboratório Associado de Sensores e Materiais (LAS), Instituto Nacional de Pesquisas Espaciais (INPE), Av. dos Astronautas 1758, São José dos Campos, 12227-010, SP, Brazil
[c] Faculdade de Ciencia e Tecnologia da Universidade de Coimbra, Rua Luis Reis Santos 3030-788, Coimbra, Portugal
[d] Instituto Pedro Nunes, Rua Pedro Nunes 3030-199, Coimbra, Portugal

ARTICLE INFO

Article history:
Received 15 December 2010
Accepted in revised form 16 July 2011
Available online 30 July 2011

Keywords:
Diamond-like carbon
Nanocrystalline diamond
Tribocorrosion
Aggressive environment

ABSTRACT

Nanocrystalline diamond (NCD) particles are incorporated into diamond-like carbon (DLC) films in order to prevent NCD-DLC electrochemical corrosion. In the current paper, tribological behavior of NCD-DLC films under aggressive solutions is discussed. DLC and NCD-DLC coated steel disks and coated and uncoated steel ball were used under rotational sliding conditions. Raman scattering spectroscopy analyzed the film's atomic arrangements and graphitization level before and after tribocorrosion tests. The NCD-DLC films confirmed to be effective in the corrosion wear resistance under corrosive environments. The results pointed that NCD-DLC films are promising corrosion protective coating in aggressive solutions for many applications.

1. Introduction

The recent interest of petroleum companies in improving the efficiency and viability of oil duct flow have been increased in the last several years [1,2]. However, commercial extraction viability has some obstacles, such as drilling of salt layer that can block and hold drill pipes. Drill and flow pipes are made with seamless steel coated with resin to decrease wear and corrosion. However, this resin wears very quickly due to the contact sliding between steel cables and inner wall of drill pipes. In addition, the corrosion of steel components due to the great pressure and the presence of sulfur dioxide decreases its efficiency and viability. Water from oil extraction generally contains high salinity, oil particles in suspension and chemicals that are added as demulsifying and defoaming [3]. The corrosive environment can result in the deposition/precipitation of corrosion products in the metal surface and increase wear inside of drill and flow pipes [3].

Candidates for the improvement of these metal surfaces may include diamond-like carbon (DLC) coatings and low temperature surface hardening [4]. DLC has been widely studied due to its mechanical properties such as low friction coefficient, high hardness, and high adherence on different substrate materials [5,6]. The combination of DLC inert characteristics to most chemicals and their amorphous structures makes them almost defect free in order to use these coatings as good candidates for oil ducts [7]. However, the presence of nanopores in DLC films can lead to the electrochemical dissolution of the substrates due to permeation of water, environmental oxygen and ions [8]. In order to improve DLC properties and applications, several authors have reported the concern of doping DLC films with silver [9,10], fluorine [11,12], silicon [13], and so on. Therefore, some of them use gas mixtures as hydrocarbon sources [11–13] and other prefers the use of a different set up to incorporate the nanoparticles [9,10]. In our previous manuscript [14], the use of DLC films with nanocrystalline diamond (NCD) particles incorporated in their structure was shown for the first time. NCD particles increased DLC electrochemical corrosion resistance, reducing its nanopores and consequently preventing aggressive ions from attacking the stainless steel surface [14,15]. The technique used was plasma enhanced chemical vapor deposition (PECVD). This is a versatile technique because different precursor gases can be used; it is easy to deposit films in samples with different sizes and shapes, and present low cost of production [16]. In the current paper, the tribological behavior of NCD-DLC films under environment air and aggressive solution was discussed. In addition, the influence of NCD particle sizes and the graphitization level before and after tribocorrosion tests was investigated.

2. Experimental procedures

The 316 L stainless steel disks (8.0 cm × 0.5 cm) were mechanically polished to a mirror-like finished surface. All the substrates were cleaned ultrasonically in an acetone bath for 15 min, and then dried in a nitrogen atmosphere. The clean samples were mounted on a water-cooled 4.8 cm diameter cathode powered by a pulsed directly current

* Corresponding author at: Instituto de Pesquisa e Desenvolvimento (IP&D), Universidade do Vale do Paraíba, Av. Shishima Hifumi 2911, São José dos Campos, SP, Brazil. Tel.: +55 12 3947 1166; fax: +55 12 3947 1149.
E-mail address: femarciano@uol.com.br (F.R. Marciano).

0257-8972/$ – see front matter © 2011 Elsevier B.V. All rights reserved.
doi:10.1016/j.surfcoat.2011.07.049

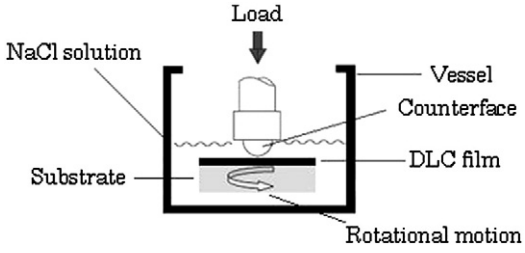

Fig. 1. Schematic diagram of a friction test in saline solution.

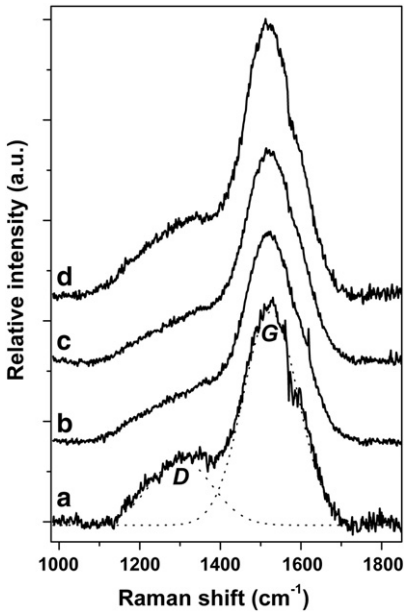

Fig. 2. Raman scattering spectra from (a) pure DLC and NCD-DLC films containing particles of (b) 4 nm, (c) 250 nm and (d) 500 nm average size. The spectra are vertically shifted for easy comparison.

plasma enhanced chemical vapor deposition power supply, with variable pulse voltage from 0 to −1000 V [6].

In the plasma chamber (vacuum base pressure of 1.3 mPa) the substrates were additionally cleaned by argon discharge with 20 sccm gas flow at 10.7 Pa working pressure and a discharge voltage of −500 V for 20 min prior to deposition. In order to enhance the adhesion of DLC film to the substrate, carbonitriding was performed before DLC deposition. The carbonitriding was carried out mixing nitrogen, hydrogen and methane gases in the proportion 12:3:1 respectively. The total flow was kept in 100 sccm at 10.7 Pa for 2 h and a discharge voltage of −560 V.

The DLC films started to be deposited using methane as the powered gas to a thickness of around 1.0 μm (20 sccm gas flow at 10.7 Pa for 2 h and a discharge voltage of −700 V). After the DLC deposition continues using hexane as the powered gas to a thickness of around 1.5 μm (at 10.7 Pa for 1 h and a discharge voltage of −700 V).

NCD particles from different average sizes (4 nm, 250 nm and 500 nm) were ultrasonic dispersed in hexane (0.5 g/L) during 10 min. These nanoparticle dispersions replaced the pure hexane during the DLC deposition to produce NCD-DLC films.

The atomic arrangement of the films was analyzed by using Raman scattering spectroscopy (Renishaw 2000 system) with an Ar^+-ion laser ($\lambda = 514$ nm) in backscattering geometry. The laser power on the sample was ~0.6 mW. The diameter of laser spot was 2.5 μm. The Raman shift was calibrated in relation to the diamond peak at 1332 cm^{-1}. All measurements were carried out in air at room temperature. The slopes of the photoluminescence background (PLB) in visible Raman spectra were used to estimate the hydrogen content in the films, following the methodology described by Casiraghi et al. [17,18]. Therefore, the NCD-DLC optical gap and density were also estimated [17,18].

A Wyko NT1100 optical profiler characterized the film topography and roughness value. The surface images were acquired in VSI (Vertical Scanning Interferometry) mode (resolution around 5 nm).

Tribological tests were done in affected environment and all characterizations were performed before and after the tests. The tests were performed on 4 mm diameter 316 L steel ball and 50 mm diameter 316 L steel flat pairs with and without DLC and NCD-DLC films. The tribological tests were carried out in dry air (42% RH) and in saline solution with 5 mass% NaCl in distilled water, with 5.6 pH at room temperature. The saline solution was prepared according to DIN 50905 norm. The substrate was embedded in saline solutions using aluminum vessel, as shown in the schematic diagram of tribotest system (Fig. 1).

The friction and wear tests were carried out by using a UMT-CETR ball-on-disk tribometer in the rotational mode with constant linear sliding speed under 10 N normal load during 1000 cycles. The tests were performed three times for each pair combination. A new position on the ball/disk was used for each test, and the friction coefficients were collected from the steady state region [19]. After the tribological tests, Raman scattering spectroscopy analysis was performed in order to study the surface changes of the films.

3. Results and discussion

Raman scattering spectroscopy was used to evaluate the chemical structure of the DLC and NCD-DLC films. Typical DLC spectra exhibit two distribution bands in the 1000–1800 cm^{-1} range, known as the *D* and *G* bands. The *D* and *G* band peak positions were determined by subtracting a linear background and fitting a Gaussian function to the peak of Raman spectrum. The peak position, width and ratio of integrated areas under *D* and *G* peaks were used to determine I_D/I_G. Fig. 2 shows the spectra from DLC and NCD-DLC films with different NCD average sizes, which are vertically shifted for easy of comparison. The main parameters obtained through the spectra (Fig. 2) are summarized in Table 1. The decrease of I_D/I_G ratio, together with the shift of *D* band's peak position towards higher frequencies, accompanied by an increase of the bandwidth is usually interpreted in terms of an increase of diamond-like domains [16,20]. Some authors reported the incorporation of metallic particles in DLC films in order to increase DLC corrosion resistance, but metallic particles promote the graphitization of amorphous carbon around them due to their catalytic

Table 1
Summarized Raman spectrum results of DLC and NCD-DLC films according to the NCD average sizes. The error represents the standard deviation of 5 different samples.

Sample	*D* band position (cm^{-1})	*G* band position (cm^{-1})	FWHM (*D*)	FWHM (*G*)	I_D/I_G	[H] (%)	Tauc gap (eV)
DLC	1301.3 ± 1.1	1522.8 ± 1.4	185.2 ± 2.8	153.6 ± 0.4	0.65 ± 0.01	34.1 ± 0.3	2.17 ± 0.03
NCD-DLC (4 nm)	1317.0 ± 2.2	1527.9 ± 0.4	243.0 ± 4.4	160.9 ± 1.6	0.50 ± 0.01	36.3 ± 0.4	2.37 ± 0.04
NCD-DLC (250 nm)	1314.9 ± 5.1	1527.1 ± 0.8	233.8 ± 7.0	159.7 ± 4.0	0.50 ± 0.01	36.6 ± 0.5	2.35 ± 0.04
NCD-DLC (500 nm)	1304.2 ± 0.5	1524.6 ± 1.0	222.9 ± 2.3	156.1 ± 1.7	0.57 ± 0.01	34.1 ± 0.7	2.17 ± 0.07

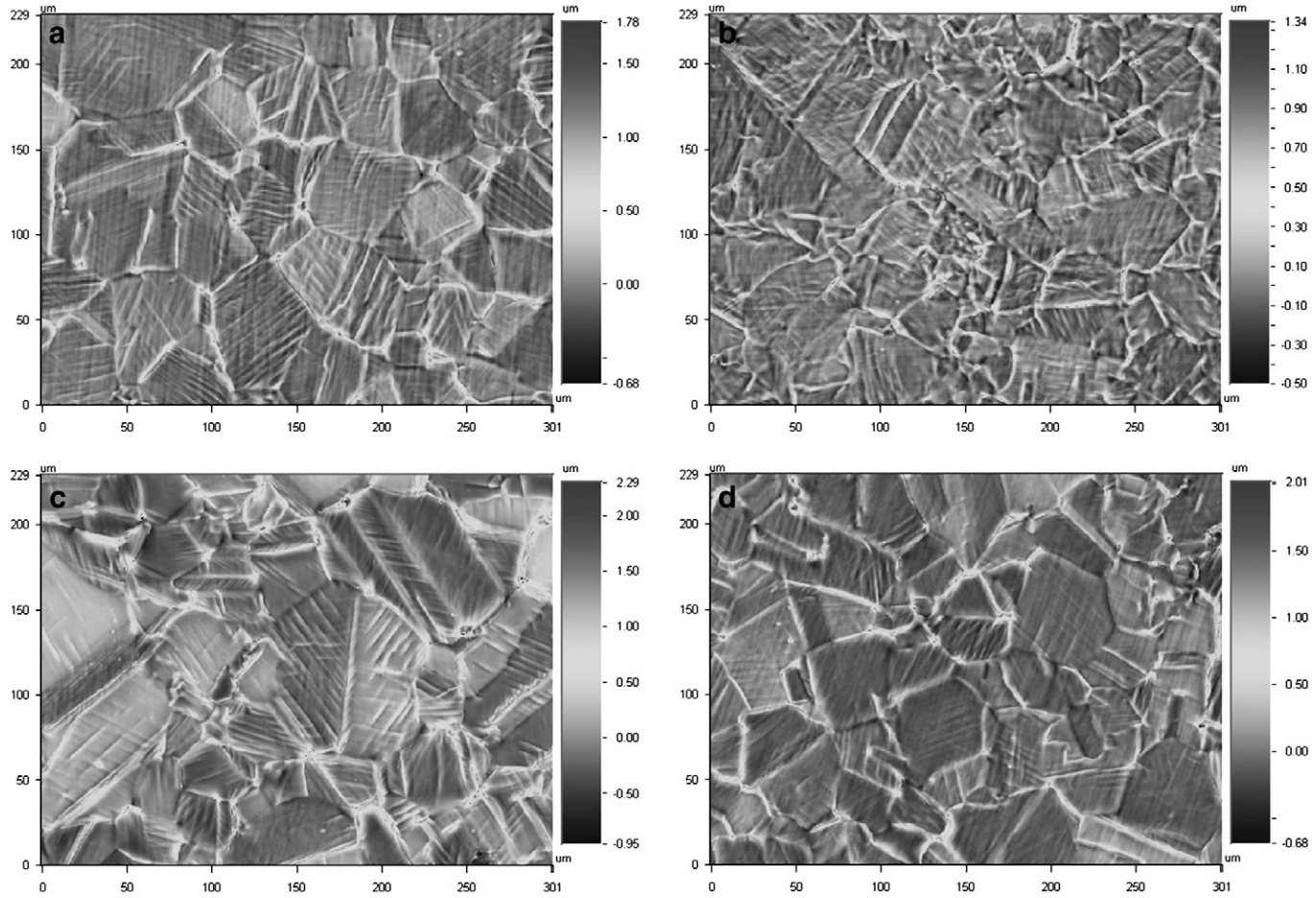

Fig. 3. Surface images of (a) DLC and NCD-DLC films containing particles of (b) 4 nm, (c) 250 nm and (d) 500 nm average size. All images acquired from optical profiler are in the amplification of 50×.

activity at high kinetic energy of the sputtered C species [21,22]. In the case of NCD-DLC films, it can be deduced that sp^3/sp^2 ratio slightly increased with the presence of NCD particles. According to Robertson [5], the sp^3 bonding confers on DLC many of the beneficial properties of diamond itself, such as its mechanical hardness, chemical and electrochemical inertness and wide band gap. The results presented here also demonstrated an increase in the film density. Note that all the characteristics obtained through Raman for NCD-DLC films are more evident in those containing small particles (4 nm of average size). This was the smaller studied size and the only size smaller than DLC average matrix (~10 nm) [6]. It suggests that minor crystalline diamond grains could occupy more nanospaces in DLC matrix, increasing its density, disorder and diamond-like characteristics.

Fig. 3 shows macroscale images from the as-deposited DLC (Fig. 3a) and NCD-DLC films (Fig. 3b–d) containing NCD particles of different average sizes. The grains seen in the images are from the carbonitriding process of stainless steel substrates. It is possible to see that in macroscale, the incorporation of NCD particles does not affect the surface appearance. The surface roughness (R_a) was measured over an area of 229 μm × 301 μm and can be seen on Table 2. The as-deposited DLC films presented roughness values around 115 nm. With the presence of bigger NCD particles (average sizes of 250 and 500 nm), the films became rougher. However, with NCD particles of 4 nm, the roughness value slightly decreased. In this case, minor nanoparticles occupying the nanospaces in DLC matrix smooth the film surface, reducing its roughness value [23].

Fig. 4 shows friction coefficient behavior of NCD-DLC films with different diamond average sizes (4 nm, 250 nm and 500 nm). These friction coefficient measurements were plotted as function of cycle numbers for 316 L stainless steel ball (a) coated and (b) uncoated with DLC, sliding against samples in dry air (42% RH) for load of 10 N and sliding speed of 120 mm s^{-1}. In the curves from DLC/DLC and DLC/NCD-DLC(250 nm) pairs (Fig. 4a), it is possible to see that the steady state starts after 500 cycles. However, DLC/NCD-DLC(4 nm) and DLC/NCD-DLC(500 nm) pairs did not show this behavior, with running-in process during almost 1000 cycles. Some authors [24,25] point out that an interfacial transfer layer is formed during the running-in stage of tribological tests. This layer may oppose a very low resistance to shear strength sliding mechanism during the steady stage [24,25]. The lowest friction in this case was around 0.07 for DLC/DLC pair. For 316 L/DLC pairs, including those with NCD particles (Fig. 4b), the friction coefficient remains between 0.18 and 0.21. This result is similar to the DLC/DLC pairs. The lowest friction coefficient was around 0.18 for 316 L/NCD-DLC(500 nm) pair.

Fig. 5 shows friction coefficient behavior of NCD-DLC films using the same parameters as described below, under 5% saline solution. In Fig. 5a, the friction coefficient reached steady state after 200 cycles for

Table 2
Surface roughness (R_a) of DLC and NCD-DLC films according to the NCD average sizes. The error represents the standard deviation of 3 different samples.

Samples	Roughness (nm)
DLC	115 ± 8
NCD-DLC (4 nm)	92 ± 7
NCD-DLC (250 nm)	216 ± 9
NCD-DLC (500 nm)	145 ± 5

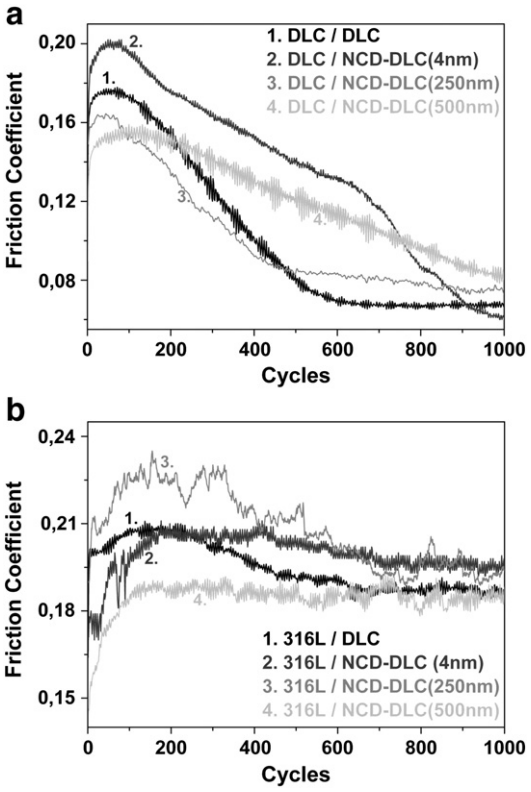

Fig. 4. Friction behavior of DLC and NCD-DLC films containing particles of 4, 250 and 500 nm average size, sliding against 316 L stainless steel ball (a) coated and (b) uncoated with DLC film, in dry air (42% RH).

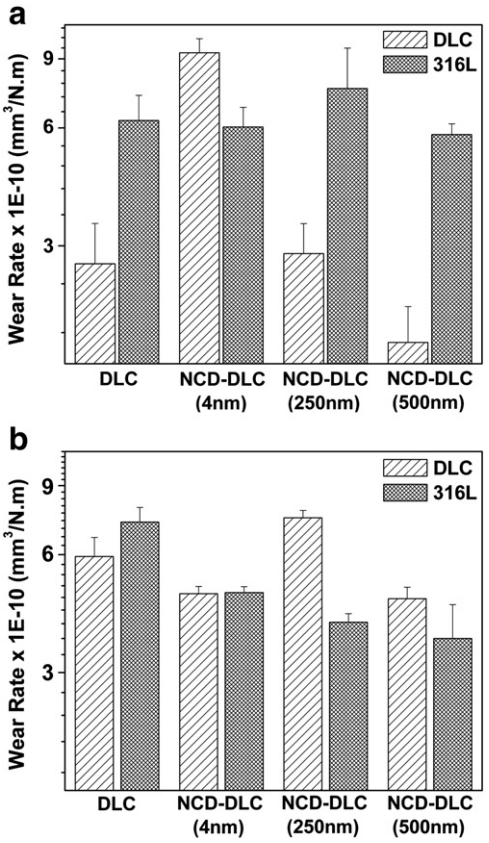

Fig. 6. Wear rate from DLC and NCD-DLC films in (a) dry air and (b) under saline solution. All the tests were performed varying the counter-body (316 L stainless steel or DLC film). The error represents the standard deviation of 3 different measurements.

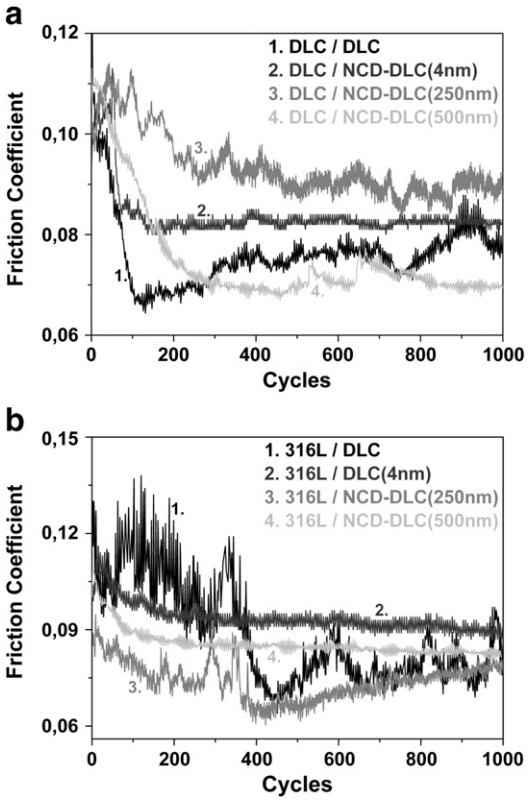

Fig. 5. Friction behavior of DLC and NCD-DLC films containing particles of 4, 250 and 500 nm average size, sliding against 316 L stainless steel ball (a) coated and (b) uncoated with DLC film, in 5% saline solution.

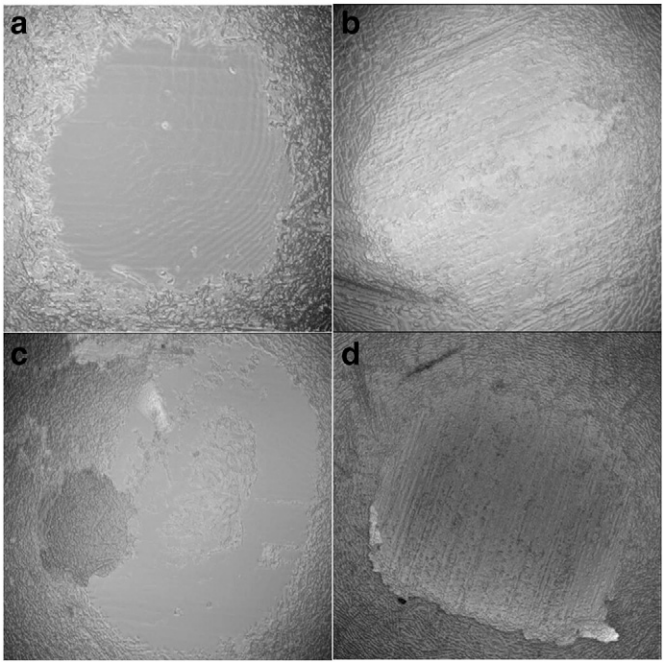

Fig. 7. Surface images of the 316 L stainless steel ball coated and uncoated with DLC films after tribological tests in air: (a) DLC/NCD-DLC(500 nm), (b) 316 L/NCD-DLC (500 nm), (c) DLC/NCD-DLC(4 nm) and (d) 316 L/NCD-DLC(250 nm) pairs. These images represent the best (a–b) and the worst (c–d) results in air. All images acquired from the optical profiler are in the amplification of 50× and represents an area of 0.069 mm^2.

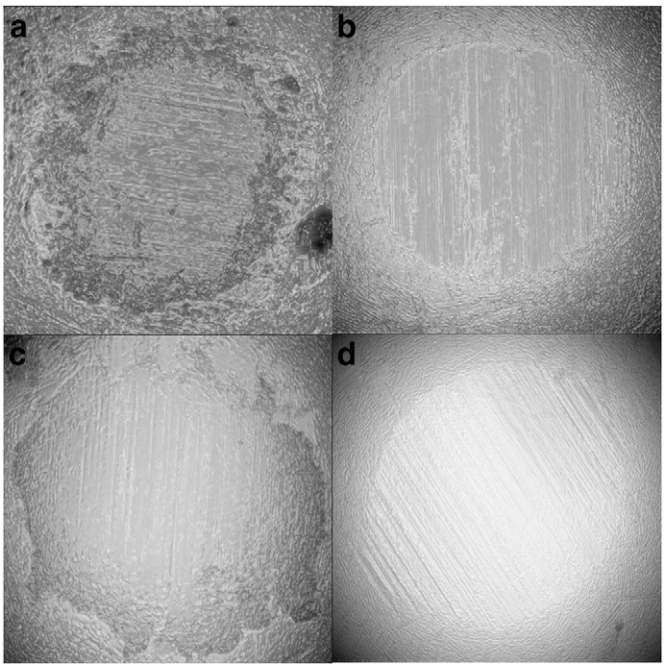

Fig. 8. Surface images of the 316 L stainless steel ball coated and uncoated with DLC films after tribological tests under saline solution: (a) DLC/NCD-DLC(500 nm), (b) 316 L/NCD-DLC(500 nm), (c) DLC/NCD-DLC(250 nm) and (d) 316 L/DLC pairs. These images represent the best (a–b) and the worst (c–d) results under saline solution. All images acquired from the optical profiler are in the amplification of 50× and represents an area of 0.069 mm^2.

all pairs. DLC/DLC and DLC/NCD-DLC(500 nm) pairs presented the lowest friction coefficient around 0.07. However, when the counter-body was changed to 316 L stainless steel, 316 L/DLC pair showed running-in process until 400 cycles and after this period, friction coefficient stabilized in 0.08, as seen in Fig. 5b. The other pairs with NCD particles showed similar behavior, without running-in period and friction coefficient between 0.07 and 0.09.

Despite being hard, NCD particles are known to have low friction coefficient [26]. When incorporated in a smooth film, like DLC, NCD-DLC friction coefficient decreases in all the samples under 5% NaCl saline solution, independently of the NCD size and the coated or uncoated counter-body. Hard coatings on a softer substrate can decrease friction and wear by preventing ploughing both on a macro and on a micro scale [27,28]. These coatings typically exhibit residual compressive stresses, which can prevent the likelihood of tensile forces occurring [29]. The reduction of friction coefficients can be explained by the formation of low-shear microfilms on the coating or perhaps only on the asperity tips of the coating [29].

Regarding the wear rate (Fig. 6), it can be seen in Fig. 6a (dry air) that the lowest wear rate was obtained from DLC/NCD-DLC(500 nm) pair, with 37% less wear than DLC/DLC pair. This result suggests that bigger particles incorporated in DLC structure helps in sliding the counter-body (in this case, DLC film). However, it is interesting to note that, when the counter-body is uncoated, the wear rate presents similar behavior. Under 5% saline solution (Fig. 6b) the 316 L/NCD-DLC (500 nm) pair showed 50% less wear rate compared to 316 L/DLC pair. When DLC film was used as the counter-body, the NCD-DLC(500 nm) also present the best result. Bigger NCD particles (500 nm) reduced contact pressure (due to increased contact area). In addition, dangling σ-bonds of surface carbon atoms by NCD particles can be mainly responsible for reduced friction and wear. These bonds can reduce the extent of adhesive interactions and hence lower friction [30]. Another factor that could explain reducing wear rates in NCD-DLC(500 nm) films is the formation of third-body from DLC wear that could fill nanospaces between bigger NCD particles (500 nm) [31].

As a comparison, Figs. 7–8 show the best and the worst results of wear tests performed in air and under saline solution, respectively. NCD-DLC(500 nm) films presented the lower wear rate independently of the counter-body, DLC (Figs. 7a and 8a) or 316 L stainless steel (Figs. 7b and 8b), and also in both environments (air and saline solution). This result is in agreement with the electrochemical corrosion tests [15] in which a superior improvement in corrosion resistance and impedance was observed due to the presence of NCD particles of 500 nm average size. In this case, NCD particles probably block the attacking of Cl^- ions, forming a barrier against the corrosion [15].

Raman spectroscopy was also performed in the track of tribological tests. Tables 3–4 show summarized Raman spectrum results of DLC and NCD-DLC films after tests in both environment according to the counter-body (DLC (Table 3) or 316 L stainless steel (Table 4)). The main factor affecting peaks position, width and intensity is the clustering of sp^2 phase [18]. The full width at half maximum of G peak, FWHM(G), and G peak position both measure disorder, however, FWHM(G) is mainly sensitive to structural disorder, while G position is mainly sensitive to topological disorder [17]. Structural disorder arises from bond angle and bond length distortions, and topological disorder arises from the size and shape distribution of sp^2 clusters [17]. These results show both G band central position and FWHM(G) shifted to higher frequencies, indicating an increase of topological and structural disorder. This increase was more evident in the pure DLC films. The wear track spectrum shows the same behavior of the film surface, indicating that the film in the track did not change its structure.

4. Conclusion

In this paper, the tribological behavior of DLC and NCD-DLC films under environment air and aggressive solution was investigated. Raman scattering spectroscopy shows NCD particles slightly increased sp^3/sp^2 ratio. The presence of bigger NCD particles increased the film roughness. These NCD particles were also demonstrated to reduce DLC friction and wear. NCD-DLC(500 nm) films presented the lowest friction coefficient and wear rate under 5% NaCl saline solution. This result suggests the potential use of these films in aggressive environment that suffers friction.

Table 3
Summarized Raman spectrum results of DLC and NCD-DLC films after tribological tests using 316 L stainless steel ball coated with DLC film as counter-body. The error represents the standard deviation of 5 different samples.

Pair of samples	Tribological environment	D band position (cm^{-1})	G band position (cm^{-1})	FWHM (D)	FWHM (G)	I_D/I_G
DLC/DLC	Air	1313.6 ± 4.2	1528.1 ± 1.4	244.8 ± 8.3	158.3 ± 1.3	0.50 ± 0.01
	NaCl solution	1314.4 ± 0.4	1528.4 ± 0.2	253.0 ± 2.0	158.9 ± 1.3	0.50 ± 0.01
DLC/NCD-DLC (4 nm)	Air	1328.1 ± 3.3	1532.4 ± 0.4	279.5 ± 2.6	160.0 ± 2.2	0.58 ± 0.02
	NaCl solution	1328.6 ± 2.8	1532.8 ± 0.8	277.0 ± 2.9	161.4 ± 0.7	0.55 ± 0.02
DLC/NCD-DLC (250 nm)	Air	1308.1 ± 1.8	1527.2 ± 0.8	234.9 ± 2.1	159.1 ± 1.8	0.50 ± 0.01
	NaCl solution	1311.1 ± 1.0	1527.0 ± 1.0	240.4 ± 10.9	158.0 ± 1.4	0.48 ± 0.05
DLC/NCD-DLC (500 nm)	Air	1319.0 ± 1.1	1529.3 ± 0.7	263.5 ± 8.6	160.5 ± 0.9	0.50 ± 0.05
	NaCl solution	1320.8 ± 2.0	1530.1 ± 0.4	263.2 ± 1.8	160.0 ± 1.6	0.48 ± 0.02

Table 4
Summarized Raman spectrum results of DLC and NCD-DLC films after tribological tests using 316 L stainless steel ball uncoated as counter-body. The error represents the standard deviation of 5 different samples.

Pair of samples	Tribological environment	*D* band position (cm^{-1})	*G* band position (cm^{-1})	FWHM (*D*)	FWHM (*G*)	I_D/I_G
316 L stainless steel/DLC	Air	1311.6 ± 4.8	1528.1 ± 1.5	242.8 ± 5.1	158.9 ± 1.6	0.49 ± 0.01
	NaCl solution	1317.1 ± 0.4	1528.7 ± 0.4	257.7 ± 1.3	157.4 ± 0.4	0.52 ± 0.01
316 L stainless steel/NCD-DLC (4 nm)	Air	1326.7 ± 2.2	1532.3 ± 0.2	276.1 ± 7.3	161.2 ± 2.2	0.56 ± 0.03
	NaCl solution	1330.5 ± 1.4	1532.9 ± 0.4	280.4 ± 6.2	161.9 ± 1.6	0.56 ± 0.03
316 L stainless steel/NCD-DLC (250 nm)	Air	1312.3 ± 2.2	1527.3 ± 0.9	233.9 ± 8.4	155.6 ± 2.0	0.49 ± 0.02
	NaCl solution	1311.1 ± 3.8	1527.6 ± 1.4	247.4 ± 8.9	158.2 ± 1.1	0.51 ± 0.03
316 L Stainless steel/NCD-DLC (500 nm)	Air	1319.0 ± 0.6	1529.4 ± 0.5	265.0 ± 17.2	160.1 ± 0.8	0.51 ± 0.08
	NaCl solution	1325.0 ± 3.5	1531.3 ± 0.9	280.7 ± 5.8	161.0 ± 1.0	0.56 ± 0.02

Acknowledgements

This study was supported by Conselho Nacional de Desenvolvimento Científico e Tecnológico (CNPq) and Fundação de Amparo à Pesquisa do Estado de São Paulo (FAPESP).

References

[1] W. Loh, R.S. Mohamed, A.C.S. Ramos, Energy Fuels 13 (1999) 323.
[2] W. Loh, A.C.S. Ramos, C.C. Delgado, R.S. Mohamed, V.R. Almeida, Pet. Sci. Technol. 17 (1999) 877.
[3] R. Allen, K. Robinson, Soc. Pet. Eng. 25549 (1993).
[4] M.S. Jellesen, T.L. Christiansen, L.R. Hilbert, P. Møller, Wear 267 (2009) 1709.
[5] J. Robertson, Mater. Sci. Eng., R 37 (2002) 129.
[6] L.F. Bonetti, G. Capote, L.V. Santos, E.J. Corat, V.J. Trava-Airoldi, Thin Solid Films 515 (2006) 375.
[7] V.J. Trava-Airoldi, G. Capote, L.F. Bonetti, J.A. Fernandes, E. Blando, R. Hübler, P.A. Radi, L.V. Santos, E.J. Corat, J. Nanosci. Nanotechnol. 9 (2009) 3891.
[8] N.W. Khun, E. Liu, X.T. Zeng, Corros. Sci. 51 (2009) 2158.
[9] F.R. Marciano, L.F. Bonetti, R.S. Pessoa, J.S. Marcuzzo, M. Massi, L.V. Santos, V.J. Trava-Airoldi, Diamond Relat. Mater. 17 (2008) 1674.
[10] F.R. Marciano, L.F. Bonetti, L.V. Santos, N.S. Da-Silva, E.J. Corat, V.J. Trava-Airoldi, Diamond Relat. Mater. 18 (2009) 1010.
[11] F.R. Marciano, D.A. Lima-Oliveira, N.S. Da-Silva, E.J. Corat, V.J. Trava-Airoldi, Surf. Coat. Technol. 204 (2010) 2986.
[12] F.R. Marciano, E.C. Almeida, D.A. Lima-Oliveira, E.J. Corat, V.J. Trava-Airoldi, Diamond Relat. Mater. 19 (2010) 537.
[13] J.R. Gomes, S.S. Camargo Jr., R.A. Simão, J.M. Carrapichano, C.A. Achete, R.F. Silva, Vacuum 81 (2007) 1448.
[14] F.R. Marciano, E.C. Almeida, L.F. Bonetti, E.J. Corat, V.J. Trava-Airoldi, J. Colloid Interface Sci. 342 (2010) 636.
[15] F.R. Marciano, E.C. Almeida, D.A. Lima-Oliveira, E.J. Corat, V.J. Trava-Airoldi, Surf. Coat. Technol. 204 (2010) 2600.
[16] V.J. Trava-Airoldi, L.F. Bonetti, G. Capote, L.V. Santos, E.J. Corat, Surf. Coat. Technol. 202 (2007) 549.
[17] C. Casiraghi, A.C. Ferrari, J. Robertson, Phys. Rev. B 72 (2005) 385.
[18] C. Casiraghi, F. Piazza, A.C. Ferrari, D. Grambole, J. Robertson, Diamond Relat. Mater. 14 (2005) 1098.
[19] O.L. Eryilmaz, A. Erdemir, Tribol. Lett. 28 (2007) 241.
[20] V.J. Trava-Airoldi, L.F. Bonetti, G. Capote, J.A. Fernandes, E. Blando, R. Hübler, P.A. Radi, L.V. Santos, E.J. Corat, Thin Solid Films 516 (2007) 272.
[21] Y. Hayashi, K.M. Krishna, H. Ebisu, T. Soga, M. Umeno, T. Jimbo, Diamond Relat. Mater. 10 (2001) 1002.
[22] C.S. Lee, T.Y. Kim, K.R. Lee, K.H. Yoon, Thin Solid Films 447–448 (2004) 169.
[23] P.A. Radi, F.R. Marciano, D.A. Lima-Oliveira, L.V. Santos, E.J. Corat, V.J. Trava-Airoldi, Appl. Surf. Sci. 257 (2011) 7387.
[24] Y. Liu, A. Erdemir, E.I. Meletis, Surf. Coat. Technol. 86–87 (1996) 564.
[25] F. Bremond, P. Fournier, F. Platon, Wear 254 (2003) 774.
[26] L. Wang, Y. Gao, Q. Xue, H. Liu, T. Xu, Mater. Sci. Eng., A 390 (2005) 313.
[27] A.A. Voevodin, J.M. Schneider, C. Rebholz, A. Matthews, Trib. Int. 29 (1996) 559.
[28] A. Erdemir, C. Bindal, G.R. Fenske, C. Zuiker, R. Csencsits, A.R. Gruen, D.M. Gruen, Diamond Films Technol. 6 (1996) 31.
[29] K. Holmberg, H. Ronkainen, A. Matthews, Ceram. Int. (2000) 787.
[30] O.L. Eryilmaz, A. Erdemir, Wear 265 (2008) 244.
[31] I.L. Singer, S.D. Dvorak, K.J. Wahl, Conference Proceedings of NordTrib Porvo, Finland, 2000.